A tree ring-based winter temperature reconstruction for the southeastern Tibetan Plateau since 1340 CE

Article *in* Climate Dynamics · February 2019

DOI: 10.1007/s00382-019-04695-3

8 authors, including:

Huang Ru
Chinese Academy of Sciences

Haifeng Zhu
Chinese Academy of Sciences

Eryuan Liang
Chinese Academy of Sciences

Bo Liu
Northwest University

Climate Dynamics
https://doi.org/10.1007/s00382-019-04695-3

A tree ring-based winter temperature reconstruction for the southeastern Tibetan Plateau since 1340 CE

Ru Huang[1,2] · Haifeng Zhu[1,3] · Eryuan Liang[1,3] · Bo Liu[4] · Jiangfeng Shi[5] · Ruibo Zhang[6] · Yujiang Yuan[6] · Jussi Grießinger[7]

Received: 11 September 2018 / Accepted: 18 February 2019

Abstract

Climatic change is exhibiting significant effects on the ecosystem of the Tibetan Plateau (TP), a climate-sensitive area. In particularly, winter frost, freezing events and snow avalanche frequently causing severe effects on ecosystem and social economy, however, few long-term winter temperature records or reconstructions hinder a better understanding on variations in winter temperature in the vast area of the TP. In this paper, we present a minimum winter (November–February) temperature reconstruction for the past 668 years based on a tree-ring network (12 new tree-ring chronologies) on the southeastern TP. The reconstruction exhibits decadal to inter-decadal temperature variability, with cold periods occurring in 1423–1508, 1592–1651, 1729–1768, 1798–1847, 1892–1927, and 1958–1981, and warm periods in 1340–1422, 1509–1570, 1652–1728, 1769–1797, 1848–1891, 1928–1957, and 1982–2007. As suggested by the comparisons with existing winter temperature series and spatial correlations with Climatic Research Unit gridded data, our reconstruction is reliable and indicative, and it can represent large-scale winter temperature variability on the southeastern TP. Furthermore, it shows an overall agreement with winter temperature from the northeastern TP on decadal to inter-decadal timescales. It also shows the possible effects of volcanic eruption and reducing solar activity on the winter temperature variability for the past six centuries on the southeastern TP.

Keywords Dendroclimatology · Southeastern Tibetan Plateau · Winter temperature · Solar activity · Volcanic eruption

1 Introduction

The Tibetan Plateau (TP) not only exerts significant influence on the large-scale atmospheric circulations (mid-latitude Westerlies and Asian Monsoon) in the Northern Hemisphere, but also provides extensive water resource for billions of human beings in Asia (Yao et al. 2013). Knowledge of its climate variability is increasingly essential for assessing its ecological and hydrological impact and the potential effect for the downstream regions. Nonetheless, meteorological observations on the TP are spatially sparse and of short length, impeding a better understanding on variations of climate change in a long-term time scale. It is thus necessary to reconstruct climate history with proxies, such as ice core, lake sediment, tree rings etc.

Tree-ring width, one of the most reliable climate proxies, is commonly used over the TP to investigate the variability of summer temperature (Liang et al. 2008, 2009; Wang et al. 2010, 2014; Zhu et al. 2011a, b), annual temperature (Wang et al. 2016; Yang et al. 2010), and annual

Electronic supplementary material The online version of this article (https://doi.org/10.1007/s00382-019-04695-3) contains supplementary material, which is available to authorized users.

✉ Haifeng Zhu
zhuhf@itpcas.ac.cn

[1] Key Laboratory of Alpine Ecology, Institute of Tibetan Plateau Research, Chinese Academy of Sciences, Beijing 100101, China

[2] University of Chinese Academy of Sciences, Beijing 10049, China

[3] CAS Center for Excellence in Tibetan Plateau Earth Sciences, Beijing 100101, China

[4] College of Urban and Environmental Sciences, Northwest University, Xi'an 710127, China

[5] School of Geographic and Oceanographic Sciences, Nanjing University, Nanjing 210023, China

[6] Institute of Desert and Meteorology, China Meteorological Administration, Urumqi 830002, China

[7] Institute of Geography, Friedrich-Alexander-University of Erlangen-Nuremberg, 91058 Erlangen, Germany

Published online: 28 February 2019

temperature cycle (Duan et al. 2017). Those valuable summer and annual temperature records not only deepen our knowledge on past climate variability, but also enhance our understanding on climate-linked glacier fluctuations and connected substantial changes in the cryosphere (Asad et al. 2017; Bräuning 2006; Hochreuther et al. 2015; Liang et al. 2009; Xu et al. 2012; Zhu et al. 2013, 2019), treeline dynamics (Liang et al. 2016; Sigdel et al. 2018), shrub recruitment (Lu et al. 2019; Wang et al. 2015), volcanic eruptions (Li et al. 2017; Liang et al. 2008; Wang et al. 2016), and historic population dynamics (Liu et al. 2009). Unfortunately, only few winter temperature reconstructions for the TP are available (Duan et al. 2017; Gou et al. 2007; Shi et al. 2017; Zhang et al. 2015c; Zhu et al. 2008). In addition, although the whole TP has experienced a uniform warming during the past century, especially since the 1960s (Kuang and Jiao 2016; Liu and Chen 2000), ice-core oxygen isotopic records showed that temperature variations of the southern part of the TP were different from these from the northern part before 20th century (Thompson et al. 2018). Such inconsistencies have also been identified by tree-ring width reconstructed drought variability on the TP (Zhang et al. 2015b). However, we know little about whether the winter temperature variability is inconsistent or consistent on the southern/northern parts of the TP on a long-term context.

The objective of this study is to develop a winter temperature (November–February) reconstruction based on a network of 12 tree-ring width chronologies. The 668-year winter temperature of this study can provide more information on long-term climate variability in the southeastern TP and the spatial variability on the northern and southern parts of TP over the past six centuries. Additionally, we also investigated the possible influence of external forcing factors (e.g., volcanic eruption and solar activity) on our winter temperature variabilities.

2 Materials and methods

2.1 Study area

Our study area is located on the southeastern TP (Fig. 1). This region is under the seasonally alternative influence of the Indian Summer Monsoon in the summer and the mid-latitude Westerlies in the winter. It is characterized by a clear transition between a humid season with monsoonal rainfall during summer (June–August) and a relatively dry

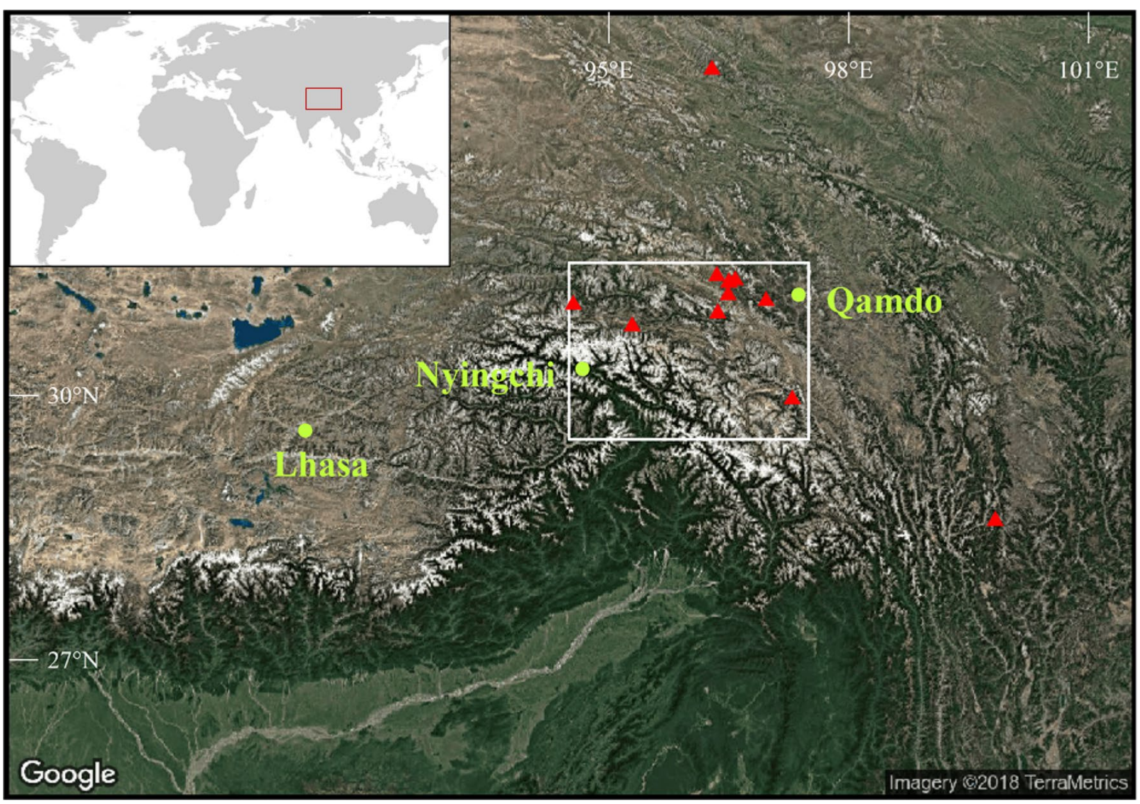

Fig. 1 Location of the 12 sampling sites used in this study on the southeastern TP (red triangles), nearby cities (Lhasa, Nyingchi, Qamdo, olive drab circles) and the selected regional CRU box (white rectangle). The T_{min} (p11–c2) in the CRU box is used for final reconstruction. The red rectangle in the inset map shows the location of our study area in the world. The background map is from http://maps.google.com/

winter season (November–February) (Fig. 1). As shown by an analysis of Climatic Research Unit (CRU) TS 4.01 data during the period 1960–2007 for the grid box 94.5–97.5°E 29.5–31.5°N, that covers most of our sampling sites (Figs. 1, 2), annual precipitation is around 550 mm, with 62% of it falling during June to August (Harris et al. 2014). The annual mean temperature is about −0.41 °C, with the warmest and coldest months being July (7.94 °C) and January (−9.46 °C), respectively. Tibetan juniper (*Sabina tibetica*) and Balfour spruce (*Picea likiangensis* var. *balfouriana*) are two dominant tree species in this region. Generally, juniper grows on the south-facing slope, and it can reach an upper distribution limit up to 4300–4600 m a.s.l.. Balfour spruce grows on north-facing slopes reaching up to ~4200–4400 m a.s.l. (Zhu et al. 2011a).

2.2 Tree-ring sites and tree-ring width (TRW) chronologies

Tree-ring samples were taken from juniper and spruce from 12 sites on the southeastern TP at elevations ranging from 4176 to 4653 m a.s.l. (red triangle in the Fig. 1; Table S1) during several field campaigns from 2007 to 2016. More than 20 trees were selected near the upper treelines with open canopy at each site. At least two cores from each tree were extracted using an increment borer with an inner diameter of 5.15 mm. Annual ring width was measured using a Lintab system with a resolution a 0.01 mm, and cross-dated with the assistance of the TSAP-win software. The COFECHA software was utilized to check the results of cross-dating (Holmes 1983). Negative exponential curve or linear regression with a negative slope was applied to remove the age-related trend for each series using the ARSTAN program (Cook 1985). The bi-weight robust mean was employed for all the detrended series to produce standard chronologies on a site-by-site basis (Fig. S1 and Fig. S2). The reliability and signal strength of each standard chronology is assessed by a 50-year moving Expressed Population Signal (EPS) with a 25-year overlap and the mean series inter-correlations (Rbar) (Fritts 1976).

2.3 Investigation of climate signals in TRW chronologies

To investigate the tree growth-climate relationships, Pearson correlation analyses were performed between each tree-ring chronology and its nearest CRU TS 4.01 gridded point data during 1960–2007. The period 1960–2007 is selected because more meteorological stations are available around our study area since 1960s, thus providing relatively reliable CRU data (Fig. S3). The monthly climate variables include total precipitation, mean temperature, maximum temperature, and minimum temperature from previous September to current October. Besides these monthly variables, a few seasonal averaged temperature and summed precipitation variables with combined months were also correlated with the chronologies. For a straightforward presentation of so many correlations between 12 individual chronologies and various climate variables, we summarized them by counting numbers of significant ($p < 0.05$) positive/negative correlations and calculating their averages, respectively.

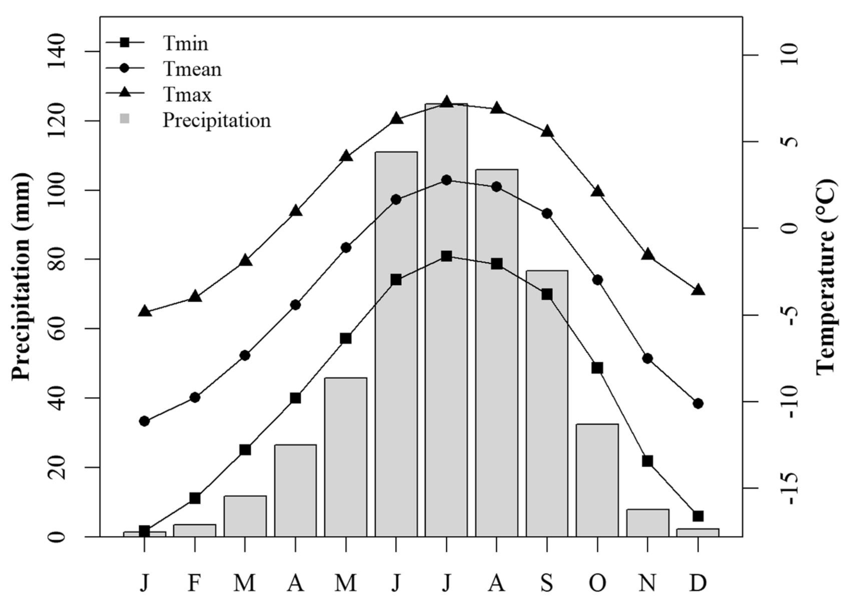

Fig. 2 The monthly CRU TS 4.01 climate variables (precipitation, minimum, maximum, and mean temperatures) during 1960–2007 from the selected regional CRU box in Fig. 1

2.4 Climate reconstruction method and calibration/verification statistics

According to the common climate signals identified by above mentioned methods, we selected a seasonal climate variable as the target for the final reconstruction. The climate variable is a regional average of CRU dataset in the spatial range of 94.5–97.5°E 29.5–31.5°N (Fig. 1, covering most of our sampling sites). To transfer the TRW chronologies to the climate target, multivariable stepwise regression analysis was performed. We firstly screened the site chronologies which had significant correlations with the reconstruction target. As there are collinearities among these selected chronologies, we did principal component analysis (PCA) on them during their common period of EPS > 0.85 to extract the PCs (principal components) which are orthogonal to each other. Then the PCs with eigenvalues > 1 were defined as the candidate predictors in the stepwise regression analysis and targeted climate variable as the predictant. As the screened chronologies (for example, n chronologies) had different lengths with EPS > 0.85, the PCA and subsequent regression analysis were performed n − 1 times as the chronologies became less and less with time further backward till to only two chronologies. Thus, totally n − 1 nested reconstructions were got after n − 1 times of regression analysis. With this iterative process, the climate target was finally extended back to 1340 CE based on as more as possible chronologies during each nested period.

Calibration and verification tests were conducted to evaluate the transfer function between reconstructed and observed temperature for each nested reconstruction. The full period 1960–2007 was split into 1960–1982 and 1983–2007, respectively as the calibration and verification periods. Then the calibration/verification periods were changed to 1984–2007 and 1960–1983, respectively for independent sub-period tests. In addition, the "leave-one-out cross-validation method" (LOOCV, Michaelsen 1987) and bootstrapping (Guiot 1991) were also performed to check the temporal stability and reliability of our models for each nested reconstruction during 1960–2007. We produced 1000 bootstrapped subsamples to calculate the models' explained variance and adjusted explained variance for each nested reconstruction. The number of each subsample was the same as the initial dataset. The statistics used here to evaluate the predictive skills of the transfer functions included the Reduction of Error (RE), Coefficient of Efficiency (CE), and explained variance. For the LOOCV technique, sign tests for both first-differenced data and raw data, RE, and the explained variance were computed to assess the consistency between the observed and reconstructed data (Fritts 1976). The RE offers a rigorous test of linkage between observed and reconstructed data, and any positive value is indicative of the good skill of the model (Fritts 1976).

Other statistical analyses were also performed to verify the final reconstruction, to investigate its spatial representativeness and periodicities. To test whether only juniper and/or spruce can provide compatible information with each other, we did reconstructions with only TRW chronologies of juniper or spruce during 1715–2007. The reconstruction methods were same as the above procedures. We also did spatial correlation analysis between reconstructed climate series and CRU TS 4.01 dataset to investigate the spatial representativeness of our reconstruction during the instrumental period (1960–2007) for each nested reconstruction. In addition, the reconstruction was compared with previously published climate reconstructions in the nearby area of the southeastern TP (Shi et al. 2017; Zhang et al. 2015c) for a validation before instrumental periods. Furthermore, the final reconstructions were compared with temperature record from the northeastern TP (Zhu et al. 2008, 400-year high-pass filtered) to investigate whether the winter temperature variabilities were consistent on the northeastern and southeastern TP during the past six centuries. The frequency features of the final reconstruction were investigated using red noise spectra (Bunn 2008) and wavelet transform (Gouhier et al. 2018). What's more, the final reconstructions were further compared to the solar activity (Delaygue and Bard 2011) to explore its possible effect on our winter temperatures. All data analyses and plots were calculated and made using R version 3.5.1 (R Core Team 2018).

3 Results

3.1 Tree growth–climate relationships and targeted climates

Winter minimum temperatures seemed to be the dominant factor influencing the tree growth in our study area. Overall, the 12 tree-ring width chronologies exhibited much stronger correlations with temperatures than with precipitation amount (summary of the correlations: Fig. 3; correlations of individual chronology for raw data: Fig. S4; correlations of individual chronology for first-differenced data: Fig. S5). Both numbers and averages of positive significant correlations with temperatures were greater than these of the negative significant correlations (Fig. 3). The averages of significant correlations ($p < 0.05$) with T_{min} were higher than these with T_{max} and T_{mean} (Fig. 3c). The highest average correlation was found with T_{min} (p11–c3) (Fig. 3c, $r = 0.46$, $p < 0.05$), which exhibited significant correlations with seven site chronologies. However, nine tree-ring width chronologies were found to correlate significantly with T_{min} (p11–c2), and average of significant correlations with T_{min} (p11–c2) was 0.43, close to the highest correlation (0.46). These significant correlations also held true for the first-differenced

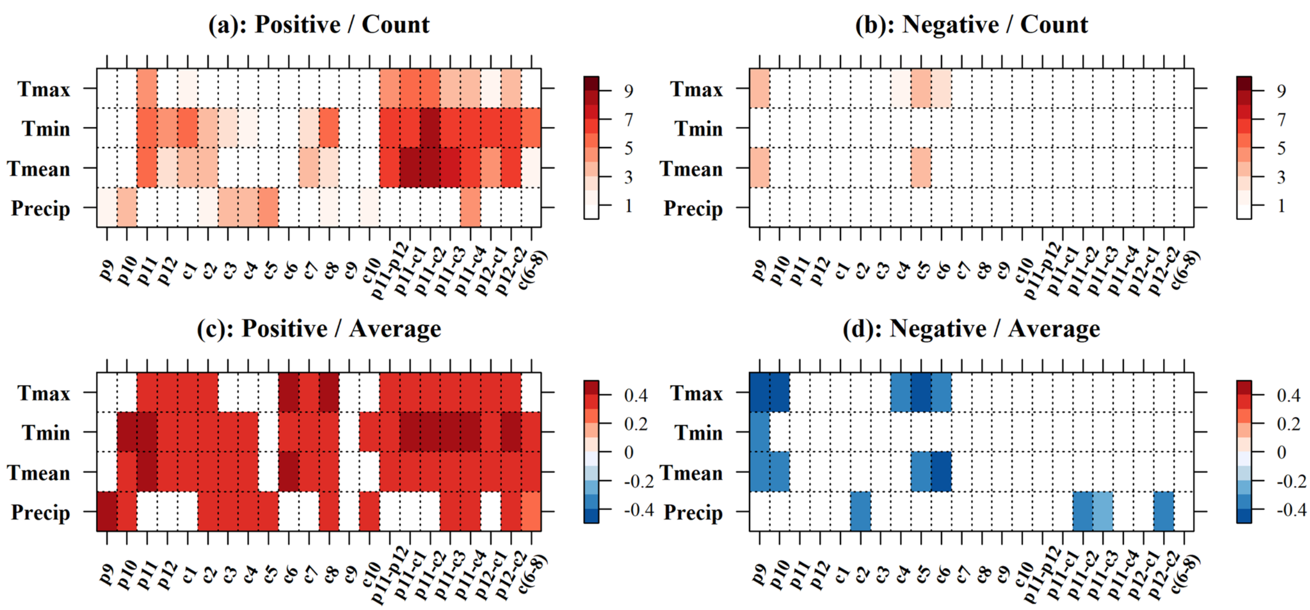

Fig. 3 Summary for the significant correlations of the 12 tree-ring width chronologies with their corresponding nearest CRU TS 4.01 gridded variables (raw data). The number and average value of the significant correlations are given for all chronologies during 1960–2007. Numbers represent months and seasons of the current 'c' and previous 'p' years. Only 95% significant correlations were displayed with color. **a, c** Positive correlations; **b, d** negative correlations; **a, b** number of the significant correlations; **b, d** average for the significant correlations

data (Fig. S5). Taken together, T_{min} (p11–c2) was considered as the targeted climate variable for final reconstruction using the nine selected tree-ring width chronologies.

3.2 Calibration/verification statistics and reconstructed temperatures

We got eight nested reconstructions (Fig. 4a), and all of them passed the calibration and validation test. The explained variance during 1960–2007 for the nested reconstructions ranged from 35.57 to 53.74% (Fig. 4a, Table S2). The RE values of each nested reconstruction during two split-up calibration and verification periods (calibration period: 1983–2007, verification period: 1960–1982; calibration period: 1960–1983, verification period: 1984–2007) were always positive (Fig. 4b), with their corresponding explained variances being present in Table S3. Both LOOCV method and bootstrap analysis yielded the almost similar explained variances for each nested reconstruction (Table S4 and Table S5). Additionally, the LOOCV also produced the positive RE (0.3–0.49) for all nested periods. The sign tests of the raw data were significant at $p < 0.01$ level, and these of the first-differenced data were not significant for all the nested reconstructions ($p > 0.05$, Table S4). These lower sign tests of the first differenced data than raw data demonstrated our reconstruction performed better in the low-frequency domains than the high-frequency domains. Moreover, for all the nested periods, the reconstructed T_{min} (p11–c2) closely matched the observed T_{min} (p11–c2) both for the raw dataset and linearly detrended datasets (Fig. 5 and Fig. S6).

Our reconstructed winter temperature proved spatially representative for each nested subset (Fig. 6 and Fig. S7). The reconstruction revealed significant correlations ($p < 0.05$) with T_{min} (p11–c2) across the south-central, and southeastern TP (1960–2007, Fig. 6a). It captured broader-scale temperature variability. The high spatial correlations mainly occurred on the southeastern TP, including Nyingchi and Qamdo of China, Bhutan, Nepal, and Myanmar. Additionally, the representativeness of our reconstructed series also held true in the high-frequency domain for the south-central, and southeastern TP (first-differenced data, Fig. 6b). Taken together, our TRW based winter temperature reconstruction represented the T_{min} (p11–c2) variability on the southeastern TP quite well.

The final reconstruction of our winter minimum temperature went back from 1340 CE to 2007 CE. The final reconstruction and eight nested reconstructions showed good coherency with one another (Fig. 4a). PCs used for each nested subset, contributions of each nest reconstruction to the final series were shown in Table S2. The finally reconstructed winter temperature exhibited decadal to interdecal variations during 1340–2007. As showed by a 51-year low-pass filtered curve (Fig. 8b), cold periods covering a multi-decadal scale occurred in 1423–1508, 1592–1651,

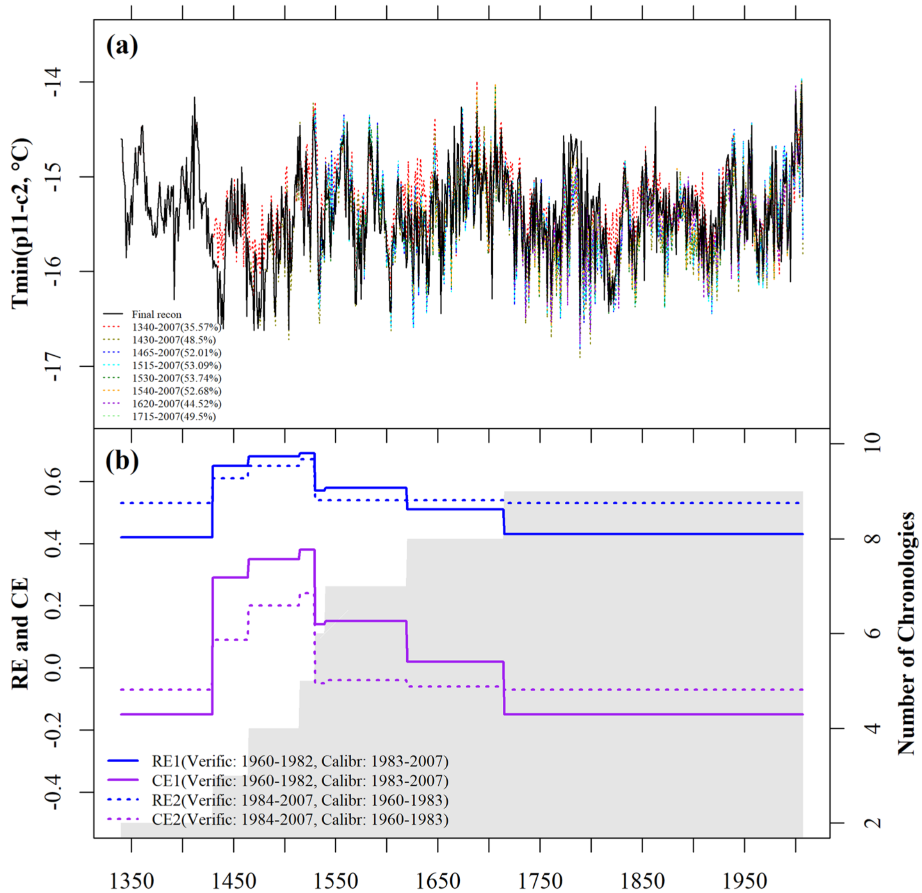

Fig. 4 **a** The final winter temperature reconstruction for the period 1340–2007 (black solid line) from different nested reconstructions (colorful dotted lines). The explained variance for each nest reconstruction during 1960–2007 is added to the legend. **b** Reduction of error (RE, blue), coefficient of efficiency (CE, purple), and the sample depth (number of chronologies for each year, grey shading). The solid lines (blue and purple) are for the RE and CE with the verification period 1960–1982, calibration period of 1983–2007, while the dotted lines (blue and purple) are for the RE and CE with the verification period of 1984–2007, calibration period of 1960–1983

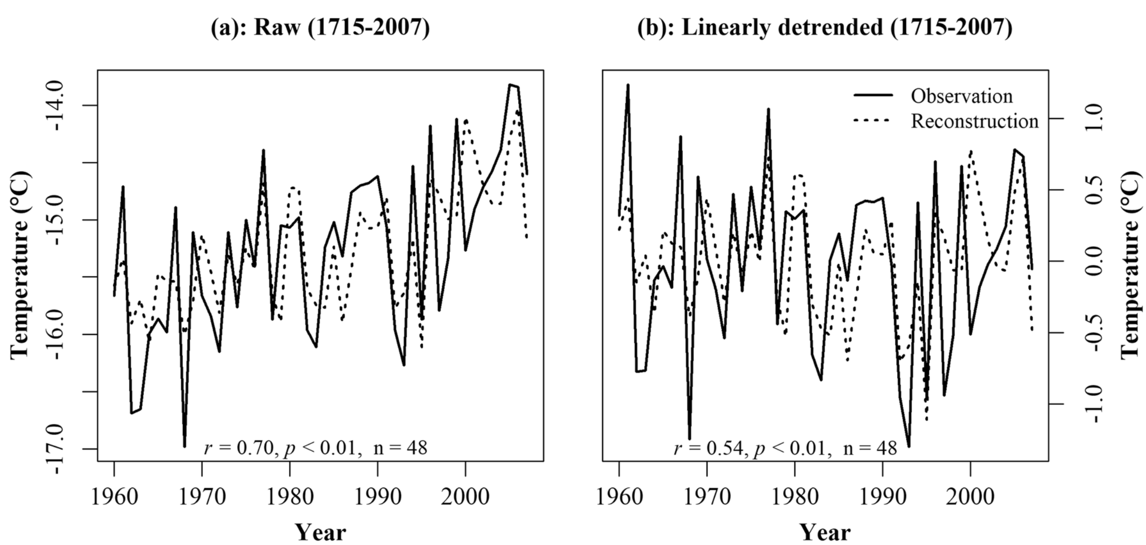

Fig. 5 Comparison of the observed and reconstructed T_{min} (p11–c2) during 1960–2007 for the nested reconstruction 1 (1715–2007). **a** Raw data; **b** linearly detrended data. Comparisons for other nested subsets are provided in the supplementary

1729–1768, 1798–1847, 1892–1927, and 1958–1981. Warm periods were in 1340–1422, 1509–1570, 1652–1728, 1769–1797, 1848–1891, 1928–1957, and 1982–2007.

Additionally, tree-ring width chronologies from mixed species within this study would result in compatible climate information. As shown in Fig. S8, the three reconstruction

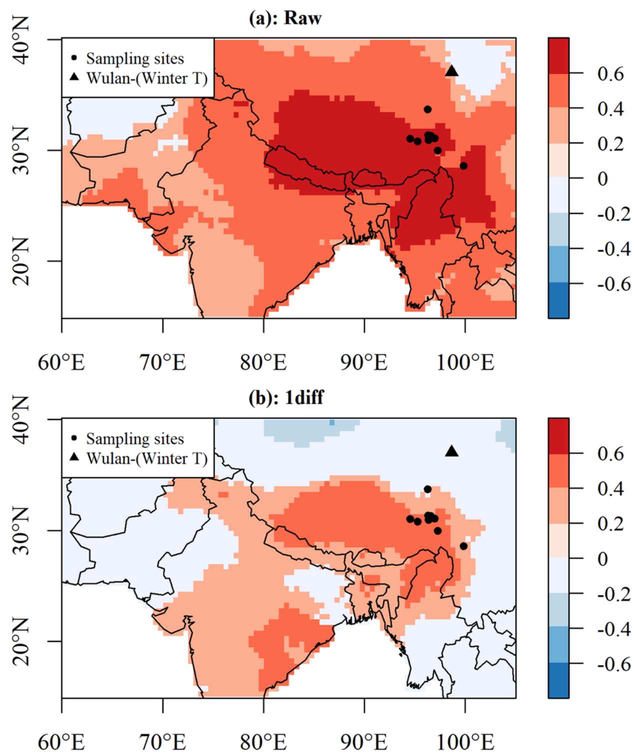

Fig. 6 Spatial correlations between our reconstruction (for the nested reconstruction 1, 1715–2007) and observed T_{min} (p11–c2) from CRU TS 4.01 during the period 1960–2007. **a** Raw data; **b** first-differenced data. Only correlations at 95% significant level are shown. Black solid circles indicate the locations of the 12 tree-ring sampling sites. Black triangle denotes the locations of the winter temperature reconstruction site on the northeastern TP (Zhu et al. 2008). Spatial correlations for other nested subsets are provided in the supplementary

chronologies (based on only juniper, only spruce, both species) exhibited good agreement during 1715–2007, implying climate reconstructions based on mixed species would provide compatible climate reconstructions.

4 Discussion

4.1 Winter temperature signals encoded in our tree-ring widths

Winter temperatures [T_{min} (p11–c3)/T_{min} (p11–c2)] appear to be a primary factor controlling tree growth at our sampling sites (Fig. 3). This is consistent with other studies from the southeastern TP (Bräuning 2006; Duan et al. 2017; Shi et al. 2017; Zhang et al. 2015c), and the northeastern TP (Gou et al. 2007; Zhang et al. 2015a; Zhu et al. 2008). Such winter temperature signals in TRW are also recorded in other areas of China, such as from central China (Cai et al. 2016; Zheng et al. 2016), southeastern China (Chen et al. 2012; Duan et al. 2012; Cai and Liu 2017; Shi et al. 2010), southwestern China (Fang et al. 2018), and northeastern China (Zhu et al. 2009). Such result also holds true for the southern Sikhote-Alin mountain range of northeastern Asia (Ukhvatkina et al. 2018), northern Iran (Bayramzadeh et al. 2018), southern Poland (Opała and Mendecki 2014), and the northeastern part of the USA (Pederson et al. 2004).

To date, there are several explanations on the possible effects of low winter temperature on subsequent tree growth. For example, colder winter can trigger bud damage, frost desiccation and reduced root activity (Körner 2012), and hence limit tree growth in the next growing season. Lower winter temperatures also lead to thicker frozen soil layers and delay of the snowmelt and spring onset date, negatively affecting tree growth (Gou et al. 2007). As a contrast, warmer winter can trigger earlier snowmelt that allows the soil layers to drain and warm quicker, and initiation of cambial activity would thus advance (Fu et al. 2012; Hollesen et al. 2015; Williams et al. 2015). These would extend the growing season length and benefit tree growth.

4.2 Validation of the reconstruction

The reliability of our winter temperature reconstruction is further confirmed by comparisons with previous winter temperature series on the southeastern TP (Shi et al. 2017; Zhang et al. 2015c, Fig. 7, Table S6). The correlations of our reconstruction with Shi et al. (2017) and Zhang et al. (2015c) for their raw data during their common periods were 0.28 ($p < 0.01$), 0.62 ($p < 0.01$), respectively (31-year high-pass filtered data: 0.28, 0.71; 31-year low-pass filtered data: 0.27, 0.45, Table S6, 1718–2006). Our winter temperature record showed an overall consistency with Shi et al. (2017) on the 40- to 70-year time scale, as detected by the wavelet coherence analysis (Fig. S9a). On annual to 32-year time scale, our series was consistent with the Zhang et al. (2015c) (Fig. S9b). Much higher consistency between our reconstruction and Zhang et al. (2015c) probably resulted from the fact that both reconstructions were derived from the same area (Qamdo), and the tree-ring width chronologies employed for final reconstructions likely shared much more common signals. The lower correlation of our chronology with Shi et al. (2017) was likely due to longer distance between these two sites (Qamdo, Shangri-La). Notably, less low-frequency (inter-decade) signals were retained by Zhang et al. (2015c) than ours, which may be attributed to the differences of age-related detrending methods. Limited inter-decade variations were retained by cubic spline detrending in Zhang et al. (2015c). These results imply more common signals of low-frequency (on inter-decadal domains) signals among these winter temperature records than those of high-frequency (on annual to decadal) signals.

In addition, comparisons with other temperature records further validated our reconstruction. Cold periods of

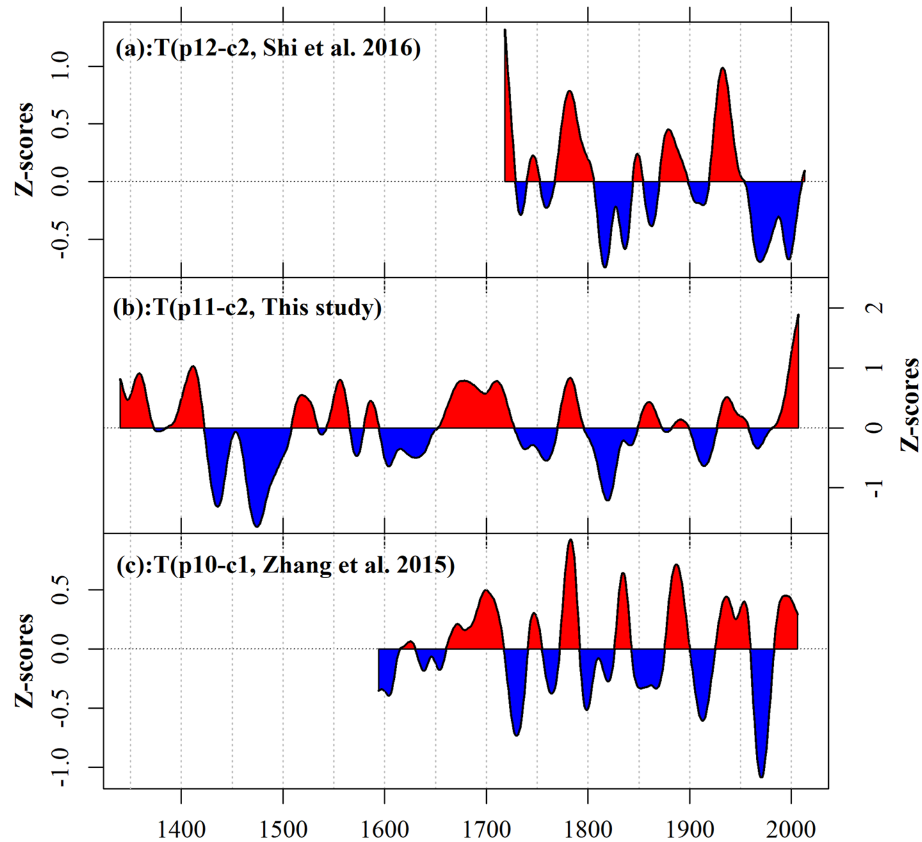

Fig. 7 Comparisons of different winter temperature reconstructions from tree rings in the southeastern Tibetan Plateau. **a** Winter temperature (p12–c2) reconstruction from the southeastern TP (Shi et al. 2017, 31-year spline low-pass filtered: shading area); **b** our winter minimum temperature (p11–c2) reconstruction on the southeastern TP 31-year spline low-pass filtered: shading area); and **c** Winter temperature (p10–c1) reconstruction from the southeastern TP (Zhang et al. 2015c, 31-year spline low-pass filtered: shading area)

1592–1656 and 1730–1769 in our reconstruction also were prevailed in the annual temperature from the southeastern TP (Wang et al. 2014). Moreover, our winter temperature chronology showed a warming trend since 1960s in southeastern TP. Such a winter warming trend was also postulated for northeastern China (Zhu et al. 2009), northeastern TP (Zhu et al. 2008), southeastern TP (Shi et al. 2017), and central China (Cai et al. 2016).

4.3 Comparison with winter temperature from the northeastern TP

Our winter temperature record of the southeastern TP is consistent with winter temperature reconstruction of Wulan from the northeast TP (Zhu et al. 2008) on decadal to multidecadal scale. Both series show high similarities (Fig. 8a, b, 400-year high-pass filtered, $r = 0.24$, $p < 0.01$). Common cold intervals were found in 1448–1508, 1600–1651, 1798–1839, 1892–1927, and 1958–1981, and common warm periods were detected in 1340–1352, 1396–1422, 1523–1570, 1671–1728, 1848–1882, and 1986–2004. In addition, as shown by the spatial correlations of our reconstructions with CRU temperature (Fig. 6 and Fig. S7), Wulan is in the domain of significant correlations only for the raw data. This implies the signals of our winter reconstruction and Wulan winter temperature share little similarity on the high-frequency domains (annual to inter-annual), and the consistency on the low-frequency domains (inter-decadal to multidecadal). The running correlations between two records with different running lengths produce the similar results (Fig. S10). These imply that common variations of winter temperature between the northeastern TP and the southeastern TP exist on decadal to multidecadal scale during the past six centuries.

Such coherency of winter temperature variability on decadal to multidecadal scale between the northeastern TP and the southeastern TP is same to the patterns identified in climate observations (Kuang and Jiao 2016; Liu and Chen 2000). However, it is different to the complicated spatial variability identified in ice-core oxygen isotopes (Thompson et al. 2018). One possible explanation is the dating uncertainties in ice cores. Another is that that ice-core oxygen isotope may showed complexity of centennial variabilities, which is longer than the decadal to multidecadal signals in this study.

4.4 Possible linkage of cold winters with external forcing

An abnormally cold interval is apparent in our reconstruction during 1810s–1820s, with a ~ 2-standard deviation in 1817 (Fig. 8b). This may be triggered by the cooling effect

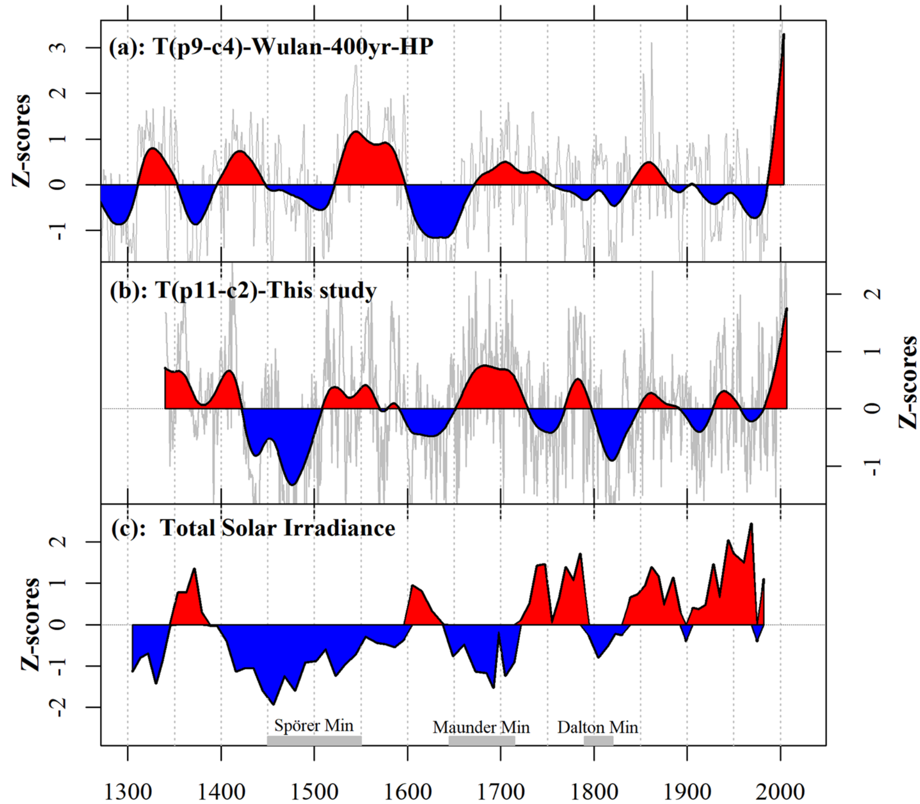

Fig. 8 Comparison of our winter temperature from the southeastern TP with winter temperature from the northeastern TP, and the solar activity. **a** Winter temperature (p9–c4) reconstruction from the northeastern TP (Wulan, 400-year high-pass filtered winter temperature series of (Zhu et al. 2008): grey line; 51-year spline for 400-year high-pass filtered series: shading area); **b** our winter minimum temperature reconstruction on the southeastern TP (p11–c2, raw data: grey line; 51-year spline for raw series: shading area); **c** total solar irradiance (TSI) during the past 600 years (Delaygue and Bard 2011), and the Spörer Minimum, Maunder Minimum and Dalton Minimum with weak solar activity are marked at the bottom

of the Tambora eruption in Indonesia in April, 1815. As the largest explosive eruption during the past 500 years (volcanic explosivity index, VEI = 7), the Tambora eruption led to a massive release of sulphur to the stratosphere, cooling the land surface by reflecting sunlight, and greatly influencing the climate in China, Europe, and America (Luterbacher and Pfister 2015; Gao et al. 2017). Similar cold intervals during 1810s–1820s have also been widely detected by reconstructed summer temperature chronologies from south-central TP (Liang et al. 2008), southeastern TP (Fan et al. 2010), Nepal (Cook et al. 2003), Bhutan (Krusic et al. 2015), East Asia (Cook et al. 2013), northern Sikkim (Borgaonkar et al. 2018), and Northern Hemisphere extra-tropics (Esper et al. 2002).

In addition, the variability of our winter temperature chronology may also be related to the solar activity. As revealed from the multi-taper spectrum and wavelet transform, our winter temperature chronology exhibited significant wavelengths of 137, 32, and 2–4 years (Fig. 9). The first two frequencies are closely linked to the solar activity (Kurths et al. 1993; Raspopov et al. 2004). The cold periods during 1460–1508, and 1800–1820 of our series correspond to weaker solar activity during the Spörer Minimum and the Dalton Minimum, respectively (Fig. 8b), further supporting the possible influence of solar activity on the winter temperature variability of the southeastern TP. However, this relationship failed during the Maunder Minimum around late seventeenth century and early eighteenth century. This may be due to mediation of internal variabilities from Atlantic Multidecadal Oscillation (AMO) (Wang et al. 2014; Shi et al. 2017), which is in a warm phase during Maunder Minimum (Gray et al. 2004). As most records in this area are around or less than 700 years, development of longer temperature reconstructions is necessary to validate this 137-year periodicity.

4.5 Comparisons with temperatures from China, Northern Hemisphere and Globe

Our winter temperature record shows similarity with the large-scale temperature reconstructions from China (Shi et al. 2012), Northern Hemisphere (Wilson et al. 2016) and Globe (Mann and Jones 2003, the 10-year spline data: Fig. 10; the 31-year spline data: Fig. S11). All records exhibited an overall warming trend since the beginning of twentieth century. Common cold periods among these records were found during 1610s, 1820s, and common warm intervals occurred during 1940s. However, discrepancies existed during 1670–1720 and before 1500. Such discrepancies may be partially due to their differing seasonality (winter/summer/annual) and methodology (detrending/reconstruction). Decreased number of available proxies before 1900s may also explain their discrepancies. More efforts (uniform seasonality and methodology, as many as possible proxies

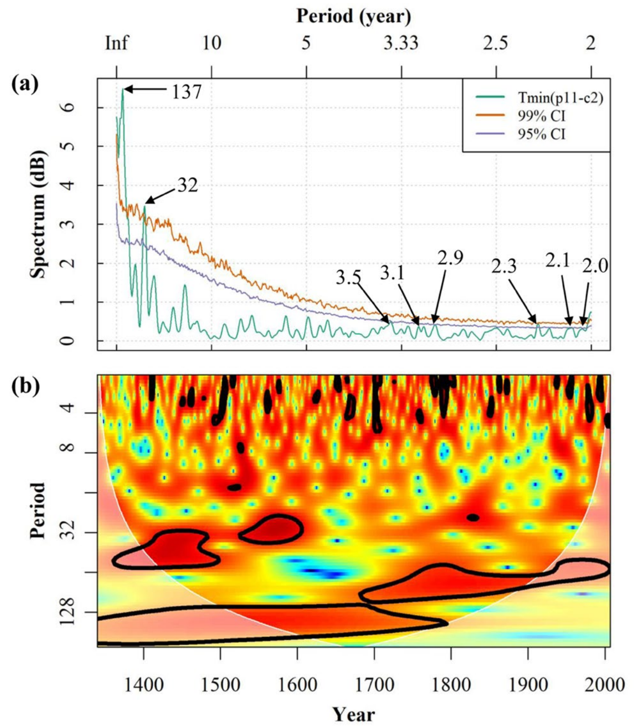

Fig. 9 **a** Multi-taper spectrum of our reconstructed winter temperature, with 95% and 99% confidence level (*CI* confidence intervals) inferred from red noise spectra, and significant periods at 95% level are marked; **b** wavelet transform of our reconstructed winter temperature, with significant periods ($p<0.05$) highlighted by solid black lines

before 1900s) are required to explore what caused these discrepancies.

5 Conclusions

Based on a network of 12 tree-ring width chronologies on the southeastern TP, we extended the winter (p11–c2) temperature record of the southeastern TP back to 1340 CE. This is by far the longest existing winter temperature reconstruction for the southeastern TP, which captures decadal to multidecadal temperature variability. Our time-series shows substantial consistency with other winter temperature reconstructions from the northeastern TP on both decadal and multidecadal scales. Additionally, our series captures a cooling effect caused by the 1815 Tambora eruption. The cold periods 1460–1508, and 1800–1820 are in good agreement with the weaker solar activity of Spörer Minimum and Dalton Minimum, respectively, implying the possible effect of reduced solar activity on our winter temperature. Considering the relative weakness of the reconstruction in high-frequency variability and less spatial coincidence, further efforts should be paid to establish more winter temperature-dominated tree-ring series to capture inter-annual signals, which will provide a more comprehensive picture of climatic history on the southeastern TP.

Fig. 10 Comparison of our winter temperature record (this study, 10-year spline, black line) with temperatures from **a** China (Shi et al. 2012, 10-year spline, red line), **b** Northern Hemisphere (Wilson et al. 2016, 10-year spline, red line) and **c** Globe (Mann and Jones 2003, 10-year spline, red line)

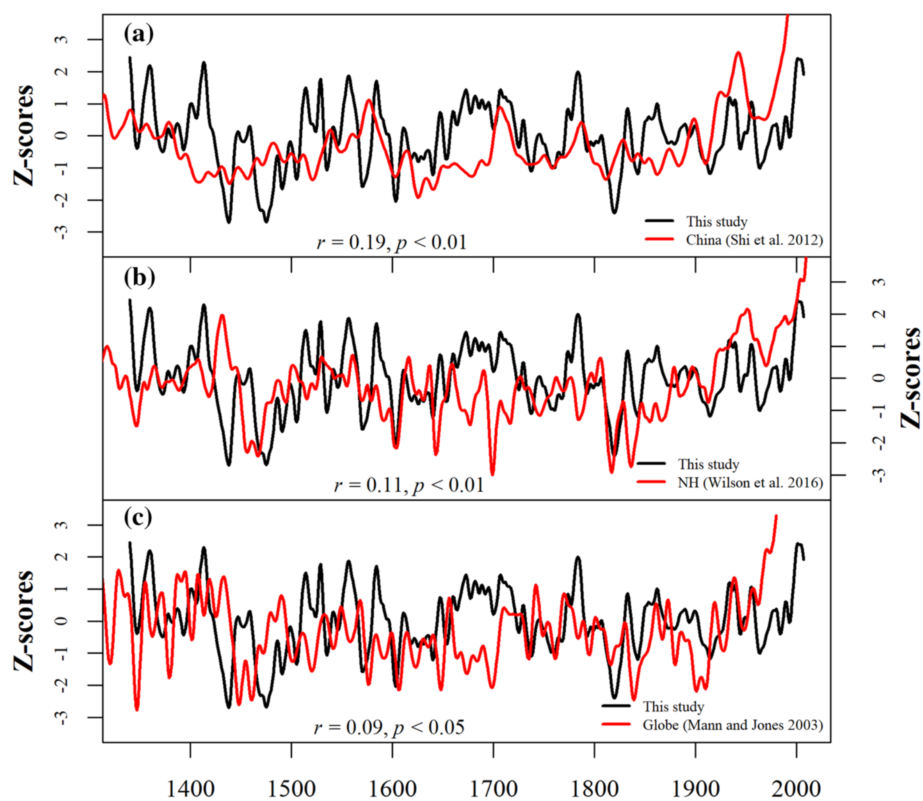

Acknowledgements This work was supported by the National Natural Science Foundation of China (Nos. 41571201, 41771240, 41661144040) and CAS "West Light Foundation" Program, and the Strategic Priority Research Program of Chinese Academy of Sciences (No. XDA20050101). Data of tree-ring width chronologies and winter temperature reconstruction in the present study are available by contacting Dr. Haifeng Zhu (zhuhf@itpcas.ac.cn). The authors declare that they have no conflict of interest.

References

Asad F, Zhu H, Zhang H et al (2017) Are Karakoram temperatures out of phase compared to hemispheric trends? Clim Dyn 48(9–10):3381–3390. https://doi.org/10.1007/s00382-016-3273-6

Bayramzadeh V, Zhu H, Lu X et al (2018) Temperature variability in northern Iran during the past 700 years. Sci Bull 63:462–464. https://doi.org/10.1016/j.scib.2018.03.011

Borgaonkar HP, Gandhi N, Ram S, Krishnan R (2018) Tree-ring reconstruction of late summer temperatures in northern Sikkim (eastern Himalayas). Palaeogeogr Palaeoclimatol Palaeoecol 504:125–135. https://doi.org/10.1016/j.palaeo.2018.05.018

Bräuning A (2006) Tree-ring evidence of "Little Ice Age" glacier advances in southern Tibet. Holocene 16(3):369–380. https://doi.org/10.1191/0959683606hl922rp

Bunn AG (2008) A dendrochronology program library in R (dplR). Dendrochronologia 26(2):115–124. https://doi.org/10.1016/j.dendro.2008.01.002

Cai Q, Liu Y (2017) Two centuries temperature variations over subtropical southeast China inferred from *Pinus taiwanensis* Hayata tree-ring width. Clim Dyn 48(5–6):1813–1825. https://doi.org/10.1007/s00382-016-3174-8

Cai Q, Liu Y, Wang Y, Ma Y, Liu H (2016) Recent warming evidence inferred from a tree-ring-based winter-half year minimum temperature reconstruction in northwestern Yichang, South Central China, and its relation to the large-scale circulation anomalies. Int J Biometeorol 60(12):1885–1896. https://doi.org/10.1007/s00484-016-1175-2

Chen F, Yuan YJ, Wei WS, Yu SL, Zhang TW (2012) Tree ring-based winter temperature reconstruction for Changting, Fujian, subtropical region of Southeast China, since 1850: linkages to the Pacific Ocean. Theor Appl Climatol 109(1–2):141–151. https://doi.org/10.1007/s00704-011-0563-0

Cook ER (1985) A time-series analysis approach to tree-ring standardization. Ph.D. dissertation, The University of Arizona, Tuson

Cook ER, Krusic PJ, Jones PD (2003) Dendroclimatic signals in long tree-ring chronologies from the Himalayas of Nepal. Int J Climatol 23(7):707–732. https://doi.org/10.1002/joc.911

Cook ER, Krusic PJ, Anchukaitis KJ, Buckley BM, Nakatsuka T, Sano M (2013) Tree-ring reconstructed summer temperature anomalies for temperate East Asia since 800 CE. Clim Dyn 41(11–12):2957–2972. https://doi.org/10.1007/s00382-012-1611-x

Delaygue G, Bard E (2011) An Antarctic view of Beryllium-10 and solar activity for the past millennium. Clim Dyn 36(11–12):2201–2218. https://doi.org/10.1007/s00382-010-0795-1

Duan J, Zhang QB, Lv L, Zhang C (2012) Regional-scale winter-spring temperature variability and chilling damage dynamics over the past two centuries in southeastern China. Clim Dyn 39(3–4):919–928. https://doi.org/10.1007/s00382-011-1232-9

Duan J, Esper J, Büntgen U et al (2017) Weakening of annual temperature cycle over the Tibetan Plateau since the 1870s. Nat Commun 8:14008. https://doi.org/10.1038/ncomms14008

Esper J, Cook ER, Schweingruber FH (2002) Low-frequency signals in long tree-ring chronologies for reconstructing past temperature variability. Science 295(5563):2250–2253. https://doi.org/10.1126/science.1066208

Fan ZX, Bräuning A, Tian QH, Yang B, Cao KF (2010) Tree ring recorded May–August temperature variations since AD 1585 in the Gaoligong Mountains, southeastern Tibetan Plateau. Palaeogeogr Palaeoclimatol Palaeoecol 296(1–2):94–102. https://doi.org/10.1016/j.palaeo.2010.06.017

Fang K, Guo Z, Chen D et al (2018) Interdecadal modulation of the Atlantic Multi-decadal Oscillation (AMO) on southwest China's temperature over the past 250 years. Clim Dyn. https://doi.org/10.1007/s00382-018-4244-x

Fritts HC (1976) Tree rings and climate. Academic, San Diego

Fu YH, Campioli M, Deckmyn G, Janssens IA (2012) The impact of winter and spring temperatures on temperate tree budburst dates: results from an experimental climate manipulation. PLoS One, 7(10):e47324. https://doi.org/10.1371/journal.pone.0047324

Gao C, Gao Y, Zhang Q, Shi C (2017) Climatic aftermath of the 1815 Tambora eruption in China. J Meteorol Res 31(1):28–38. https://doi.org/10.1007/s13351-017-6091-9

Gou X, Chen F, Jacoby G, Cook E, Yang M, Peng J, Zhang Y (2007) Rapid tree growth with respect to the last 400 years in response to climate warming, northeastern Tibetan Plateau. Int J Climatol 27(11):1497–1503. https://doi.org/10.1002/joc.1480

Gouhier TC, Grinsted A, Simko V (2018) R package biwavelet: conduct univariate and bivariate wavelet analyses (Version 0.20.17). Available from https://github.com/tgouhier/biwavelet

Gray ST, Graumlich LJ, Betancourt JL, Pederson GT (2004) A tree-ring based reconstruction of the Atlantic Multidecadal Oscillation since 1567 AD. Geophys Res Lett 31(12):L12205. https://doi.org/10.1029/2004GL019932

Guiot J (1991) The bootstrapped response function. Tree-Ring Bull 51:39–41

Harris I, Jones PD, Osborn TJ, Lister DH (2014) Updated high-resolution grids of monthly climatic observations-the CRU TS3.10 Dataset. Int J Climatol 34:623–642. https://doi.org/10.1002/joc.3711

Hochreuther P, Loibl D, Wernicke J, Zhu H, Grießinger J, Bräuning A (2015) Ages of major Little Ice Age glacier fluctuations on the southeast Tibetan Plateau derived from tree-ring-based moraine dating. Palaeogeogr Palaeoclimatol Palaeoecol 422:1–10. https://doi.org/10.1016/j.palaeo.2015.01.002

Hollesen J, Buchwal A, Rachlewicz G, Hansen BU, Hansen MO, Stecher O, Elberling B (2015) Winter warming as an important co-driver for *Betula nana* growth in western Greenland during the past century. Glob Change Biol 21(6):2410–2423. https://doi.org/10.1111/gcb.12913

Holmes RL (1983) Computer-assisted quality control in tree-ring dating and measurement. Tree-Ring Bull 43:69–75

Körner C (2012) Alpine treelines: functional ecology of the global high elevation tree limits. Springer Science Business Media, New York

Krusic PJ, Cook ER, Dukpa D, Putnam AE, Rupper S, Schaefer J (2015) Six hundred thirty-eight years of summer temperature variability over the Bhutanese Himalaya. Geophys Res Lett 42(8):2988–2994. https://doi.org/10.1002/2015GL063566

Kuang X, Jiao JJ (2016) Review on climate change on the Tibetan Plateau during the last half century. J Geophys Res Atmos 121:3979–4007. https://doi.org/10.1002/2015JD024728

Kurths J, Spiering C, Müller-Stoll W, Triegler U (1993) Search for solar periodicities in Miocene tree ring widths. Terra Nova 5(4):359–363

Li M, Huang L, Yin ZY, Shao X (2017) Temperature reconstruction and volcanic eruption signal from tree-ring width and maximum latewood density over the past 304 years in the southeastern

Tibetan Plateau. Int J Biometeorol 61(11):2021–2032. https://doi.org/10.1007/s00484-017-1395-0

Liang E, Shao X, Qin N (2008) Tree-ring based summer temperature reconstruction for the source region of the Yangtze River on the Tibetan Plateau. Glob Planet Change 61(3–4):313–320. https://doi.org/10.1016/j.gloplacha.2007.10.008

Liang E, Shao X, Xu Y (2009) Tree-ring evidence of recent abnormal warming on the southeast Tibetan Plateau. Theor Appl Climatol 98(1–2):9–18. https://doi.org/10.1007/s00704-008-0085-6

Liang E, Wang Y, Piao S et al (2016) Species interactions slow warming-induced upward shifts of treelines on the Tibetan Plateau. Proc Natl Acad Sci USA 113(16):4380–4385. https://doi.org/10.1073/pnas.1520582113

Liu X, Chen B (2000) Climatic warming in the Tibetan Plateau during recent decades. Int J Climatol 20(14):1729–1742. https://doi.org/10.1002/1097-0088(20001130)20:14<1729::AID-JOC556>3.0.CO;2-Y

Liu Y, An Z, Linderholm HW et al (2009) Annual temperatures during the last 2485 years in the mid-eastern Tibetan Plateau inferred from tree rings. Chin Sci Bull 52(3):348–359. https://doi.org/10.1007/s11430-009-0025-z

Lu X, Liang E, Wang Y, Babst F, Leavitt S, Camarero JJ (2019) Past the climate optimum: recruitment is declining at the world's highest juniper shrublines on the Tibetan Plateau. Ecology 100(2):e02557. https://doi.org/10.1002/ecy.2557

Luterbacher J, Pfister C (2015) The year without a summer. Nat Geosci 8(4):246. https://doi.org/10.1038/ngeo2404

Mann ME, Jones P (2003) Global surface temperatures over the past two millennia, Geophys Res Lett, 30(15):1820. https://doi.org/10.1029/2003GL017814

Michaelsen J (1987) Cross-validation in statistical climate forecast models. J Clim Appl Meteorol 26:1589–1600

Opała M, Mendecki MJ (2014) An attempt to dendroclimatic reconstruction of winter temperature based on multispecies tree-ring widths and extreme years chronologies (example of Upper Silesia, Southern Poland). Theor Appl Climatol 115(1–2):73–89. https://doi.org/10.1007/s00704-013-0865-5

Pederson N, Cook ER, Jacoby GC, Peteet DM, Griffin KL (2004) The influence of winter temperatures on the annual radial growth of six northern range margin tree species. Dendrochronologia 22(1):7–29. https://doi.org/10.1016/j.dendro.2004.09.005

R Core Team (2018) R: a language and environment for statistical computing. R Foundation for Statistical Computing, Vienna. https://www.R-project.org/

Raspopov OM, Dergachev VA, Kolström T (2004) Periodicity of climate conditions and solar variability derived from dendrochronological and other palaeoclimatic data in high latitudes. Palaeogeogr Palaeoclimatol Palaeoecol 209(1–4):127–139. https://doi.org/10.1016/j.palaeo.2004.02.022

Shi J, Cook ER, Lu H, Li J, Wright WE, Li S (2010) Tree-ring based winter temperature reconstruction for the lower reaches of the Yangtze River in southeast China. Clim Res 41(2):169–175. https://doi.org/10.3354/cr00851

Shi F, Yang B, Von Gunten L (2012) Preliminary multiproxy surface air temperature field reconstruction for China over the past millennium. Sci China Earth Sci 55(12):2058–2067

Shi S, Li J, Shi J, Zhao Y, Huang G (2017) Three centuries of winter temperature change on the southeastern Tibetan Plateau and its relationship with the Atlantic Multidecadal Oscillation. Clim Dyn 49(4):1305–1319. https://doi.org/10.1007/s00382-016-3381-3

Sigdel SR, Wang Y, Julio Camarero J, Zhu H, Liang E, Peñuelas J (2018) Moisture-mediated responsiveness of treeline shifts to global warming in the Himalayas. Glob Change Biol 24(11):5549–5559. https://doi.org/10.1111/gcb.14428

Thompson LG, Yao T, Davis ME, Mosley-Thompson E, Wu G, Porter SE et al (2018) Ice core records of climate variability on the Third Pole with emphasis on the Guliya ice cap, western Kunlun Mountains. Quat Sci Rev 188:1–14. https://doi.org/10.1016/j.quascirev.2018.03.003

Ukhvatkina ON, Omelko AM, Zhmerenetsky AA, Petrenko TY (2018) Autumn–winter minimum temperature changes in the southern Sikhote-Alin mountain range of northeastern Asia since 1529 AD. Clim Past 14:57–71. https://doi.org/10.5194/cp-14-57-2018

Wang L, Duan J, Chen J, Huang L, Shao X (2010) Temperature reconstruction from tree-ring maximum density of Balfour spruce in eastern Tibet, China. Int J Climatol 30(7):972–979. https://doi.org/10.1002/joc.2000

Wang J, Yang B, Qin C, Kang S, He M, Wang Z (2014) Tree-ring inferred annual mean temperature variations on the southeastern Tibetan Plateau during the last millennium and their relationships with the Atlantic Multidecadal Oscillation. Clim Dyn 43(3–4):627–640. https://doi.org/10.1007/s00382-013-1802-0

Wang Y, Liang E, Ellison AM, Lu X, Camarero JJ (2015) Facilitation stabilizes moisture-controlled alpine juniper shrublines in the central Tibetan Plateau. Glob Planet Change 132:20–30. https://doi.org/10.1016/j.gloplacha.2015.06.007

Wang B, Chen T, Xu G, Wu G, Li C (2016) Reconstructed annual mean temperatures for the northeastern margin of the Tibetan Plateau: associations with the East Asian monsoons and volcanic events. Int J Climatol 37(6):3044–3056. https://doi.org/10.1002/joc.4900

Williams CM, Henry HA, Sinclair BJ (2015) Cold truths: how winter drives responses of terrestrial organisms to climate change. Biol Rev 90(1):214–235. https://doi.org/10.1111/brv.12105

Wilson R, Anchukaitis K, Briffa KR et al (2016) Last millennium northern hemisphere summer temperatures from tree rings: part I: the long term context. Quat Sci Rev 134:1–18. https://doi.org/10.1016/j.quascirev.2015.12.005

Xu P, Zhu H, Shao X, Yin Z (2012) Tree ring-dated fluctuation history of Midui glacier since the Little Ice Age in the southeastern Tibetan Plateau. Chin Sci Bull 55(4):521–529. https://doi.org/10.1007/s11430-011-4338-3

Yang B, Kang X, Liu J, Bräuning A, Qin C (2010) Annual temperature history in Southwest Tibet during the last 400 years recorded by tree rings. Int J Climatol 30(7):962–971. https://doi.org/10.1002/joc.1956

Yao T, Masson-Delmotte V, Gao J et al (2013) A review of climatic controls on $\delta^{18}O$ in precipitation over the Tibetan Plateau: observations and simulations. Rev Geophys 51(4):525–548. https://doi.org/10.1002/rog.20023

Zhang H, Shao X, Zhang Y (2015a) Which climatic factors limit radial growth of Qilian juniper at the upper treeline on the northeastern Tibetan Plateau? J Geogr Sci 25(10):1173–1182. https://doi.org/10.1007/s11442-015-1226-3

Zhang QB, Evans MN, Lyu L (2015b) Moisture dipole over the Tibetan Plateau during the past five and a half centuries. Nat Commun 6:8062. https://doi.org/10.1038/ncomms9062

Zhang RB, Yuan YJ, Wei WS et al (2015c) Dendroclimatic reconstruction of autumn-winter mean minimum temperature in the eastern Tibetan Plateau since 1600 AD. Dendrochronologia 33:1–7. https://doi.org/10.1016/j.dendro.2014.09.001

Zheng Y, Shao X, Lu F, Li Y (2016) February–May temperature reconstruction based on tree-ring widths of *Abies fargesii* from the Shennongjia area in central China. Int J Biometeorol 60(8):1175–1181. https://doi.org/10.1007/s00484-015-1111-x

Zhu H, Zheng Y, Shao X, Liu X, Xu Y, Liang E (2008) Millennial temperature reconstruction based on tree-ring widths of Qilian juniper from Wulan, Qinghai Province, China. Chin Sci Bull 53(24):3914–3920. https://doi.org/10.1007/s11434-008-0400-8

Zhu H, Fang X, Shao X, Yin Z (2009) Tree ring-based February-April temperature reconstruction for Changbai Mountain in Northeast China and its implication for East Asian winter monsoon. Clim Past 5(4):661–666. https://doi.org/10.5194/cp-5-661-2009

Zhu H, Shao X, Yin Z, Huang L (2011a) Early summer temperature reconstruction in the eastern Tibetan Plateau since AD 1440 using tree-ring width of *Sabina tibetica*. Theor Appl Climatol 106(1–2):45–53. https://doi.org/10.1007/s00704-011-0419-7

Zhu H, Shao X, Yin Z, Xu P, Xu Y, Tian H (2011b) August temperature variability in the southeastern Tibetan Plateau since AD 1385 inferred from tree rings. Palaeogeogr Palaeoclimatol Palaeoecol 305(1–4):84–92. https://doi.org/10.1016/j.palaeo.2011.02.017

Zhu H, Xu P, Shao X, Luo H (2013) Little Ice Age glacier fluctuations reconstructed for the southeastern Tibetan Plateau using tree rings. Quat Int 283:134–138. https://doi.org/10.1016/j.quaint.2012.04.011

Zhu H, Shao X, Zhang H, Asad F, Sigdel S, Huang R, Li Y, Liu W, Muhammad S, Hussain I, Grießinger J, Liang E (2019) Trees record changes of the temperate glaciers on the Tibetan Plateau: potential and uncertainty. Glob Planet Change 173:15–23. https://doi.org/10.1016/j.gloplacha.2018.12.004

Publisher's Note Springer Nature remains neutral with regard to jurisdictional claims in published maps and institutional affiliations.